Materials Advances

ROYAL SOCIETY OF CHEMISTRY

COMMUNICATION

View Article Online
View Journal | View Issue

Cite this: *Mater. Adv.*, 2021, 2, 7379

Received 19th July 2021,
Accepted 3rd October 2021

DOI: 10.1039/d1ma00624j

rsc.li/materials-advances

Enhancing charge separation in conjugated microporous polymers for efficient photocatalytic hydrogen evolution†

Zhuangfei Qian,[a] Yajie Yan,[a] Ziqi Liang,[a] Xiaodong Zhuang[b] and Kai A. I. Zhang*[a]

The fast recombination of photogenerated electron–hole pairs after charge separation is one of the main factors limiting the achievement of high efficiency of organic semiconductor photocatalysts. Herein, we report a conjugated microporous polymer (CMP)/graphene heterosystem for enhanced photocatalytic hydrogen evolution. Benzothiadiazole-based CMPs were synthesized on graphene sheets *Via* covalent bonds. Owing to the substantially enhanced charge separation and transfer within the organic semiconductor/conductor heterostructure, the heterosystems exhibited increased photocatalytic hydrogen evolution rates up to 977 μmol g^{-1} h^{-1}, which is approximately two times as high as that of bulk CMP.

Conjugated polymers are emerging organic heterogeneous photocatalysts due to their attractive metal-free nature, chemical stability and diverse structures.[1–6] In recent years, enormous efforts have been made to promote their photocatalytic performance by enhancing their light-harvesting ability, facilitating the charge separation and transfer efficiency, tuning the morphology, improving the hydrophilicity, *etc.*[7–11] The fast recombination of the photogenerated electron–hole pair is one of the main limiting factors for the photocatalytic applications of single component semiconductor photocatalysts. Recent studies revealed several methods to promote the charge separation and transfer efficiency inside the photocatalyst material.[12–14] For example, doping of heteroatoms, variation of substitution or spatial configuration,[3,15,16] adjustment of electron-donor and -acceptor combinations,[17–20] and construction of conjugated polymer/metal heterostructures have been reported.[21–23]

Among the reported optimization methods, the construction of heterostructures could substantially enhance the charge separation and transfer efficiency of the semiconductor materials. Upon light irradiation, the excited electron in the conduction band (CB) of the semiconductor can be spontaneously transferred to the conductor without a significant energy barrier. The photoexcited electron–hole pair can then be spatially separated, and their fast recombination possibly surpassed. As a facile method to facilitate the charge separation and transfer inside photocatalysts, designing heterostructure-based photocatalytic systems, especially inorganic and metal-containing semiconductor/conductor systems, has been a research focus in recent years. Nevertheless, pure non-metal heterostructure systems have barely been designed for polymer-based photocatalysts.

As a potential candidate for non-metal conductor materials, graphene possesses unique features such as high work function (4.42 eV),[24–26] ultrafast theoretical charge carrier mobility (2×10^5 cm^2 V^{-1} s^{-1} at room temperature),[27,28] high electrical conductivity (10^6 S cm^{-1})[28] and solution-processable nature. These properties make graphene a promising candidate for photocatalytic semiconductor/conductor heterostructures. So far, most of the reported catalytic materials containing graphene were hybrid materials consisting of metal oxides.[29–32] Conjugated polymer/graphene systems have rarely been studied. Therefore, an investigation in this specific class of photocatalytic systems is of necessity.

Here, we report conjugated microporous polymer (CMP)/graphene heterostructures for visible light-driven photocatalytic hydrogen evolution. The photogenerated charge separation and transfer within CMP/graphene heterostructures are substantially enhanced by varying the content of graphene. Specifically, the CMP/graphene heterostructure containing 0.5 wt% graphene exhibits enhanced photocatalytic H_2 evolution rates up to 977 μmol g^{-1} h^{-1}, which was approximately two times as high as that of bulk CMP. This work provides a simple and facile method for improving the photocatalytic hydrogen evolution performance of conjugated polymer photocatalysts.

In order to form covalent bonds between graphene and the CMPs, 4-bromophenyl-modified graphene (Br-graphene) sheets

[a] *Department of Materials Science, Fudan University, Songhu Road 2005, Shanghai 200438, China. E-mail: kai_zhang@fudan.edu.cn*
[b] *School of Chemistry and Chemical Engineering, Shanghai Jiao Tong University, Dongchuan Road 800, Shanghai 200240, China*

† Electronic supplementary information (ESI) available. See DOI: 10.1039/d1ma00624j

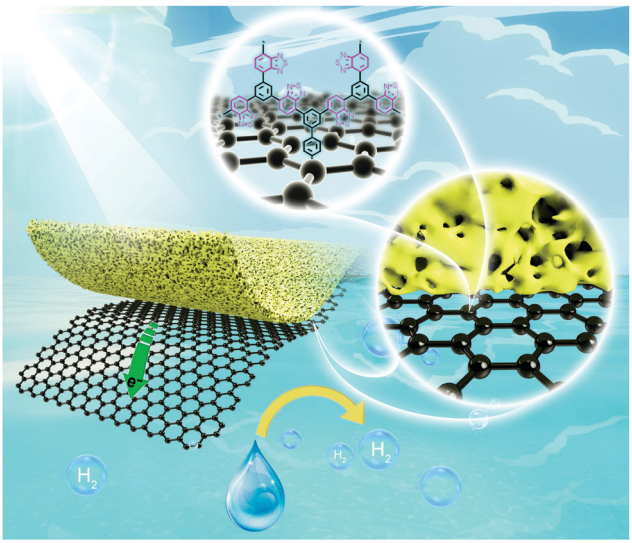

Scheme 1 Illustration of the facilitated charge transfer across the graphene/polymer heterostructures for enhanced photocatalytic hydrogen evolution.

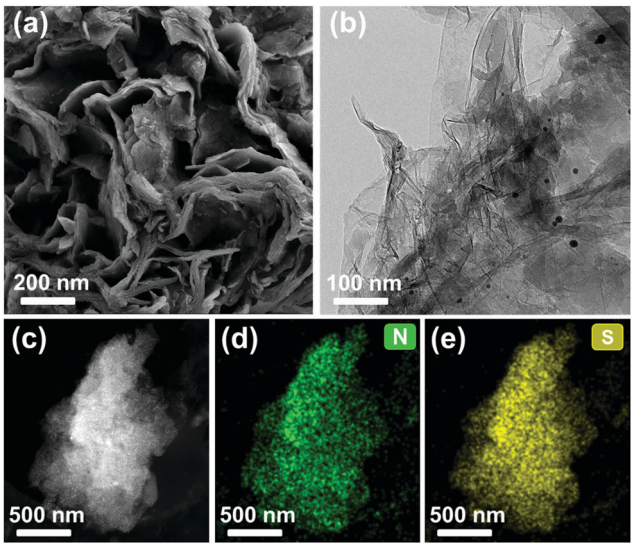

Fig. 1 (a) SEM, (b) TEM and (c) HAADF-STEM images of GMP-0.5; the corresponding elemental mapping images of (d) nitrogen and (e) sulfur.

were prepared *via* a radical substitution method according to a previous report.[33] As shown in Scheme 1, 4,7-dibromo-2,1,3-benzothiadiazole and 1,3,5-phenyltriboronic acid were polymerized directly onto the surface of Br-graphene *via* a Suzuki–Miyaura cross-coupling reaction, resulting in a series of graphene-containing microporous polymers (GMPs). The mass ratio of Br-graphene was adjusted from 0.1 to 5 wt%. The resulted CMP/graphene materials were referred to as GMP-*x*, in which *x* is the weight percentage of graphene. Compared to the bulk CMP, CMP-BT was directly synthesized from the polymerization of 1,3,5-phenyltriboronic acid and 4,7-dibromo-2,1,3-benzothiadiazole without graphene.

The obtained materials showed colors ranging from dark yellow to black with increasing content of graphene (0–5 wt%). All products were insoluble in the common solvents tested. The morphologies of CMP-BT and GMP-*x* were characterized by scanning electron microscopy (SEM) and transmission electron microscopy (TEM). Differing from the bulk material, CMP-BT with a fused particle-like structure, all the graphene-containing GMPs showed a sheet-like morphology, as shown in Fig. 1a and b, with GMP-0.5 as an example. The elemental mapping images indicated that nitrogen and sulfur atoms were evenly distributed on the particles (Fig. 1c and d). No free CMP particles were found, which suggests the successful synthesis of CMPs on the graphene surface (Fig. S1–S4, ESI†). The porous properties of GMPs and CMP-BT were characterized by nitrogen adsorption/desorption measurements (Fig. S5 and S6, ESI†). CMP-BT showed a type I sorption isotherm for a typical microporous character. The Brunauer–Emmett–Teller (BET) surface area of CMP-BT was calculated to be 237 $m^2 g^{-1}$. With the incorporation of graphene sheets, GMP-0.1 (277 $m^2 g^{-1}$) yielded a slightly higher BET surface area than CMP-BT. The BET surface areas decreased with increasing graphene content, with GMP-5 showing a rather non-porous character. The physical properties of the materials are listed in Table 1.

The solid-state ^{13}C cross-polarization magic angle spinning (CP-MAS) NMR spectra of the materials showed a peak at 155 ppm, which was characteristic of carbon atoms adjacent to the nitrogen atoms of benzothiadiazole (BT) motifs (Fig. S7–S12, ESI†). The signals between 128 and 137 nm can be assigned to the sp^2-hybridized carbon atoms of 1,3,5-functionalized phenyl linkers and BT units. The fused peaks indicated the presence of highly crosslinked structures in the polymer skeleton. The typical stretching vibration modes of N–S and C=N on BT units at 1550 and 1350 cm^{-1} were also observed using a Fourier transform infrared (FT-IR) spectrometer (Fig. S13, ESI†).

According to the UV-vis diffusion reflectance (DR) spectra, CMP-BT exhibited the narrowest adsorption range up to 490 nm. Benefitting from the introduction of graphene, GMPs showed a wider visible light adsorption range which extended to nearly 700 nm (Fig. 2a). The blue-shifted adsorption maximum can be ascribed to the increasing content of graphene. The reason might be that the addition of graphene might lead to more phenyl content within the conjugated system *via* the C–C coupling reaction during the polymerization process, thereby shifting the energy of the heterostructures to a higher level. The same phenomenon could be observed by the emission maxima of GMPs in the photoluminescence (PL) spectra (Fig. 2b). For GMP-1, 3, and 5, the attenuated photoluminescence emission revealed an overall stronger luminescence quenching with increasing graphene content, which suggests that the radiative recombination was retarded with improved charge separation.

For a deeper investigation of the impact of graphene on the photophysical properties, the materials were characterized by time-resolved photoluminescence (TRPL) spectroscopy (Fig. 2c). The double-exponential fitting results were calculated and are summarized in Table S1 (ESI†). It was found that all

Table 1 Physical properties and photocatalytic hydrogen evolution rates of CMP-BT and the GMPs

Sample	Bandgap (opt.)[a] (eV)	HOMO[b]/LUMO[c] (V *vs.* NHE)	S_{BET}[d] ($m^2\ g^{-1}$)	Pore volume[d] ($cm^3\ g^{-1}$)	HER[e] ($\mu mol\ h^{-1}\ g^{-1}$)
CMP-BT	2.2	1.49/−0.71	237	0.26	497
GMP-0.1	2.0	1.28/−0.72	277	0.38	492
GMP-0.5	2.1	1.4/−0.70	195	0.39	977
GMP-1	1.7	0.92/−0.78	35	0.27	616
GMP-3	1.8	1.05/−0.75	27.6	0.21	503
GMP-5	1.8	1.03/−0.77	2.0	0.01	380

[a] Derived from the adsorption edges. [b] Calculated by extracting the lowest unoccupied molecular orbital (LUMO) level from the optical bandgap. [c] Determined by cyclic voltammetry. [d] Calculated from the N_2 sorption isotherms. [e] The photocatalytic hydrogen evolution was conducted using 20 mg photocatalyst, 100 mL water, 10 mL TEOA and 3 wt% Pt co-catalyst.

GMPs showed shorter average fluorescence lifetimes than CMP-BT (τ_{avg} = 1.73 ns). GMP-0.1, 0.5, and 1 with graphene contents less than or equal to 1 wt% showed average lifetimes of about 1.50, 1.48 and 1.51 ns, respectively. The lifetime for GMP-5 significantly reduced to 0.60 ns. Moreover, GMP-0.1 and 0.5 exhibited longer τ_1 lifetimes than CMP-BT (0.59 ns). The τ_1 proportions of GMP-0.1 and 0.5 increased compared with CMP-BT, while the τ_2 proportion decreased. The shorter fluorescence lifetime and the attenuated PL emission indicated that, with enhanced electron transport between CMP and graphene within the heterostructures, a non-radiative charge transfer pathway might have been activated.[34–36]

Photocurrent measurements revealed the stronger transient light responses of GMP-0.1 and GMP-0.5 than that of CMP-BT, indicating an improved photo-induced electronic conductivity for the GMPs (Fig. 2d). By further increasing the graphene contents for GMP-1 to GMP-3, the materials showed weaker photocurrent responses. This could be caused by the rather dominant conducting character of the heterostructure. On the basis of the photophysical results, graphene could act as an electron mediator for improved charge separation and transfer efficiency in the CMP/graphene heterostructures, thus likely further improving their photocatalytic performances.

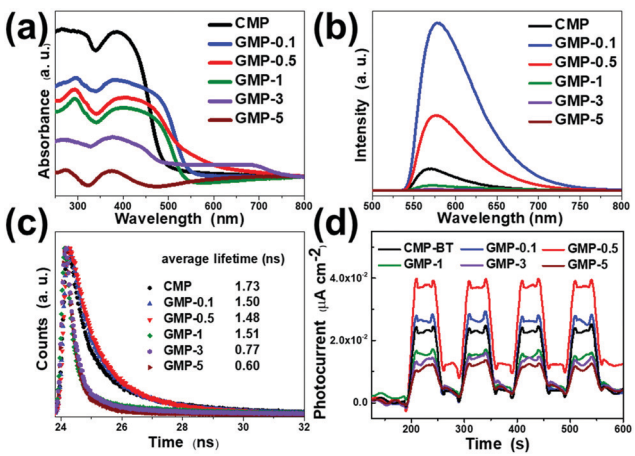

Fig. 2 (a) UV-Vis DRS spectrum of GMPs and CMP-BT. (b) Steady-state photoluminescence and (c) time-resolved PL curves excited at 460 nm of CMP and all GMPs as indicated. (d) Photocurrent response spectra of GMPs and CMP-BT upon visible light irradiation (λ > 420 nm).

We then tested the photocatalytic activity of the CMP/graphene heterostructures for visible light-driven hydrogen evolution (λ > 420 nm). The average H_2 production rates of the photocatalysts with varying content of graphene are shown in Fig. 3a. The hydrogen evolution rate (HER) of the GMPs increased first from 482 to 977 $\mu mol\ g^{-1}\ h^{-1}$, then decreased with the increasing content of graphene. Among them, CMP-BT exhibited a HER of 497 $\mu mol\ g^{-1}\ h^{-1}$, which was comparable to our previous reported value.[16] A similar HER of about 482 $\mu mol\ g^{-1}\ h^{-1}$ was achieved by GMP-0.1, which is likely because of the negligible influence of a minimum load of graphene (0.1 wt%) toward the optical and electronic properties. The highest HER was achieved by GMP-0.5. The HER of GMP-0.5 (977.1 $\mu mol\ g^{-1}\ h^{-1}$) was about two times as high as that of CMP-BT. The results showed that the construction of CMP/graphene could effectively facilitate the charge transfer and inhibit the recombination of photoinduced electron and hole pairs. The photocatalytic hydrogen evolution activity decreased when the graphene content was further increased to 1.0 wt%. GMP-5, with the largest graphene content (5 wt%) among the as-prepared photocatalysts, achieved the lowest HER (380 $\mu mol\ g^{-1}\ h^{-1}$). The decreasing activity from GMP-1 to GMP-5 could be ascribed to the blocked charge transfer via defect recombination caused by a higher graphene content since defects were inevitably formed during the chemical processing of graphene. Hence, it was more likely to occur in systems with excess amounts of graphene. The decreased photocatalytic efficiency with excessive graphene in heterostructures was observed by Cui *et al.* in TiO_2/graphene composites.[31] The apparent quantum efficiency (AQE) of GMP-0.5 as the best performing photocatalyst was calculated under the irradiation of visible light with selected wavelength (Fig. 3b), which was consistent with the visible-light adsorption spectrum of GMP-0.5. The AQE at 420 nm was calculated to be 0.36%. The repeating experiments showed that the amount of evolved H_2 increased linearly in each cycle (Fig. 3c). A slight decay in the second cycle was likely caused by the consumption of TEOA, and it was recovered after addition of TEOA as a sacrificial reagent. No discernible composition change of the photocatalyst was found after the repeated experiments, as shown in the FT-IR and UV-vis spectra (Fig. S13 and S14, ESI†), indicating the long-term photo- and structural stability of the GMPs. Additionally, it is worth noting that no relationship was found between the residual Pd and photocatalytic activity of the as-prepared photocatalysts according to the ICP-MS results (Table S2, ESI†).

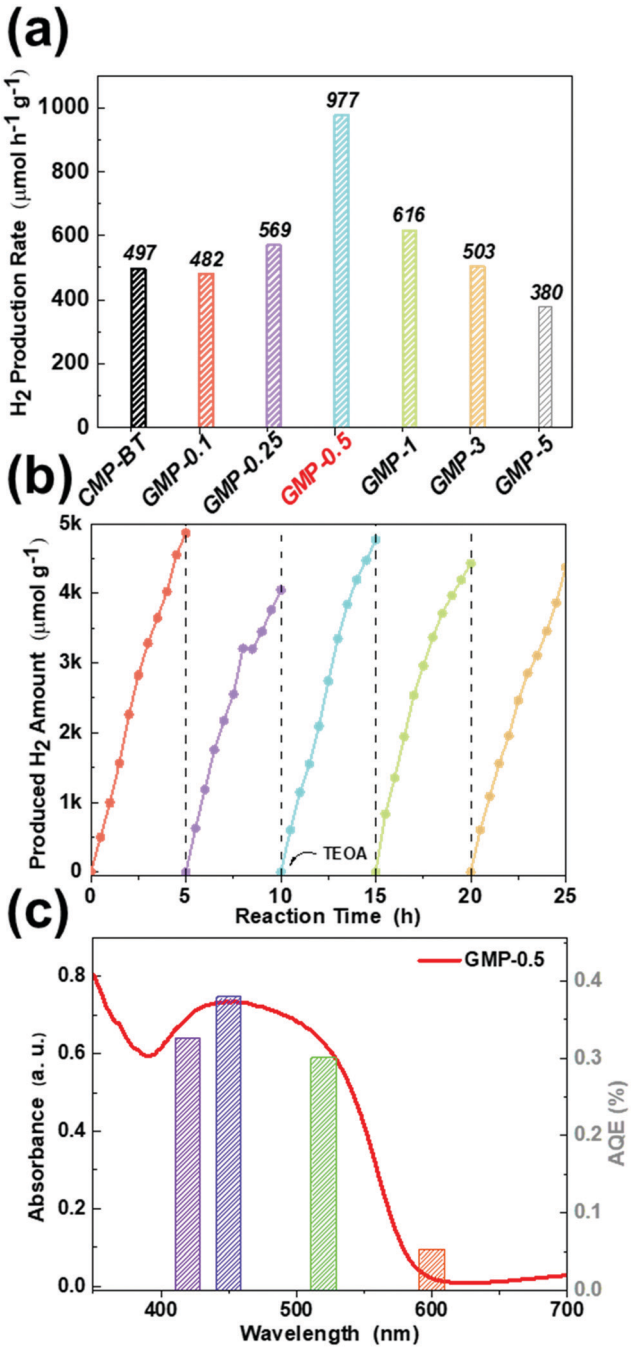

Fig. 3 (a) Photocatalytic H_2 production rates of CMP-BT and GMPs under visible light irradiation ($\lambda > 420$ nm). (b) Recycling test of GMP-0.5. (c) Apparent quantum efficiencies of photocatalytic H_2 evolution with GMP-0.5 as the photocatalyst in relation to irradiation wavelength.

Conclusions

In conclusion, we have designed CMP/graphene heterostructures as photocatalysts for visible light-driven H_2 evolution by direct synthesis of CMPs on graphene sheets *via* covalent bonds. By adjusting the graphene content, the charge separation and transfer ability of the resulted heterostructures could be modified. The heterostructure with 0.5 wt% graphene content showed the highest photocatalytic H_2 generation efficiency within the series of materials, which is approximately two times as high as that of bulk CMP. The design strategy of metal-free heterostructures could offer a flexible and feasibly way for photocatalytic efficiency enhancement by facilitating the charge transfer ability.

Conflicts of interest

The authors declare no conflicts of interest.

Acknowledgements

The authors acknowledge Fudan University for funding.

Notes and references

1 L. Wang, J. Byun, R. Li, W. Huang and K. A. I. Zhang, *Adv. Synth. Catal.*, 2018, **360**, 4312–4318.
2 X. Wang, Y. Shi, R. W. Graff, D. Lee and H. Gao, *Polymer*, 2015, **72**, 361–367.
3 Z. J. Wang, K. Garth, S. Ghasimi, K. Landfester and K. A. I. Zhang, *ChemSusChem*, 2015, **8**, 3459–3464.
4 A. H. Lu, G. P. Hao, Q. Sun, X. Q. Zhang and W. C. Li, *Macromol. Chem. Phys.*, 2012, **213**, 1107–1131.
5 Y. Bai, L. Wilbraham, B. J. Slater, M. A. Zwijnenburg, R. S. Sprick and A. I. Cooper, *J. Am. Chem. Soc.*, 2019, **141**, 9063–9071.
6 R. S. Sprick, J. X. Jiang, B. Bonillo, S. Ren, T. Ratvijitvech, P. Guiglion, M. A. Zwijnenburg, D. J. Adams and A. I. Cooper, *J. Am. Chem. Soc.*, 2015, **137**, 3265–3270.
7 D. Taylor, S. J. Dalgarno, Z. Xu and F. Vilela, *Chem. Soc. Rev.*, 2020, **49**, 3981–4042.
8 F. Vilela, K. Zhang and M. Antonietti, *Energy Environ. Sci.*, 2012, **5**, 7819–7832.
9 Y. Xu, S. Jin, H. Xu, A. Nagai and D. Jiang, *Chem. Soc. Rev.*, 2013, **42**, 8012–8031.
10 J. S. M. Lee and A. I. Cooper, *Chem. Rev.*, 2020, **120**, 2171–2214.
11 J. X. Jiang, Y. Li, X. Wu, J. Xiao, D. J. Adams and A. I. Cooper, *Macromolecules*, 2013, **46**, 8779–8783.
12 Z. Qian and K. A. I. Zhang, *Sol. RRL*, 2021, **5**, 1–23.
13 C. Ayed, L. Caire Da Silva, D. Wang and K. A. I. Zhang, *J. Mater. Chem. A*, 2018, **6**, 22145–22151.
14 L. Lin, Z. Lin, J. Zhang, X. Cai, W. Lin, Z. Yu and X. Wang, *Nat. Catal.*, 2020, **3**, 649–655.
15 Y. S. Kochergin, D. Schwarz, A. Acharjya, A. Ichangi, R. Kulkarni, P. Eliášová, J. Vacek, J. Schmidt, A. Thomas and M. J. Bojdys, *Angew. Chem., Int. Ed.*, 2018, **57**, 14188–14192.
16 C. Yang, B. C. Ma, L. Zhang, S. Lin, S. Ghasimi, K. Landfester, K. A. I. Zhang and X. Wang, *Angew. Chem., Int. Ed.*, 2016, **55**, 9202–9206.
17 Z. A. Lan, G. Zhang, X. Chen, Y. Zhang, K. A. I. Zhang and X. Wang, *Angew. Chem., Int. Ed.*, 2019, **58**, 10236–10240.

18 Z.-A. Lan, M. Wu, Z. Fang, X. Chi, X. Chen, Y. Zhang and X. Wang, *Angew. Chem., Int. Ed.*, 2021, **60**, 16355–16359.
19 C. Yang, W. Huang, L. C. da Silva, K. A. I. Zhang and X. Wang, *Chem. – Eur. J.*, 2018, **24**, 17454–17458.
20 Z. Wang, X. Yang, T. Yang, Y. Zhao, F. Wang, Y. Chen, J. H. Zeng, C. Yan, F. Huang and J. X. Jiang, *ACS Catal.*, 2018, **8**, 8590–8596.
21 G. Mukherjee, J. Thote, H. B. Aiyappa, S. Kandambeth, S. Banerjee, K. Vanka and R. Banerjee, *Chem. Commun.*, 2017, **53**, 4461–4464.
22 L. Wang, X. Zheng, L. Chen, Y. Xiong and H. Xu, *Angew. Chem., Int. Ed.*, 2018, **57**, 3454–3458.
23 S. Wang, X. Yang, H. Hou, X. Ding, S. Li, F. Deng, Y. Xiang and H. Chen, *Catal. Sci. Technol.*, 2017, **7**, 418–426.
24 K. S. Novoselov, A. K. Geim, S. V. Morozov, D. Jiang, M. I. Katsnelson, I. V. Grigorieva, S. V. Dubonos and A. A. Firsov, *Nature*, 2005, **438**, 197–200.
25 A. A. Balandin, *Nat. Mater.*, 2011, **10**, 569–581.
26 R. R. Nair, P. Blake, A. N. Grigorenko, K. S. Novoselov, T. J. Booth, T. Stauber, N. M. R. Peres and A. K. Geim, *Science*, 2008, **320**, 1308.
27 X. Du, I. Skachko, A. Barker and E. Y. Andrei, *Nat. Nanotechnol.*, 2008, **3**, 491–495.
28 Z. S. Wu, W. Ren, L. Gao, J. Zhao, Z. Chen, B. Liu, D. Tang, B. Yu, C. Jiang and H. M. Cheng, *ACS Nano*, 2009, **3**, 411–417.
29 Z. Chen, S. Yang, Z. Tian and B. Zhu, *Appl. Surf. Sci.*, 2019, **469**, 657–665.
30 A. Iwase, Y. H. Ng, Y. Ishiguro, A. Kudo and R. Amal, *J. Am. Chem. Soc.*, 2011, **133**, 11054–11057.
31 X. Y. Zhang, H. P. Li, X. L. Cui and Y. Lin, *J. Mater. Chem.*, 2010, **20**, 2801–2806.
32 G. Williams, B. Seger and P. V. Kamt, *ACS Nano*, 2008, **2**, 1487–1491.
33 X. Zhuang, F. Zhang, D. Wu, N. Forler, H. Liang, M. Wagner, D. Gehrig, M. R. Hansen, F. Laquai and X. Feng, *Angew. Chem., Int. Ed.*, 2013, **52**, 9668–9672.
34 D. Kozawa, X. Zhu, Y. Miyauchi, S. Mouri, M. Ichida, H. Su and K. Matsuda, *J. Phys. Chem. Lett.*, 2014, **5**, 1754–1759.
35 L. Ke, P. Li, X. Wu, S. Jiang, M. Luo, Y. Liu, Z. Le, C. Sun and S. Song, *Appl. Catal., B*, 2017, **205**, 319–326.
36 L. Gaudreau, K. J. Tielrooij, G. E. D. K. Prawiroatmodjo, J. Osmond, F. J. G. De Abajo and F. H. L. Koppens, *Nano Lett.*, 2013, **13**, 2030–2035.